Orbit Analysis at the TTF Linac Using Model Independent Methods

P. Castro, M. Seidel

February 5, 2002

Abstract

Model independent analysis (MIA) can be used in linear accelerators to analyse large statistical samples of orbit data in order to address questions like number of jittering variables that affect the beam, residual dispersion, and resolution of beam position monitors. We describe the application of MIA to TTF and try to answer some questions of practical interest.

1 Principles of Model Independent Analysis

A detailed description of the theory can be found in the paper by John Irwin et al. [1]. The basic principles will be described here as far as they are needed for the analysis of the TTF measurements.

Due to rather general reasons position measurements at different beam position monitors (BPM's) in a beamline must be correlated in certain ways. For example a betatron oscillation will result in well defined orbit amplitude ratios at the different BPM's. The correlations can be revealed just by applying statistical methods to a set of BPM measurements, and without knowledge of the underlying physical model. In the simplest case the accelerator is operated in stable conditions and orbits for a large number of pulses are recorded. The "natural" beam jitter, for example caused by laser beam position jitter in the gun, charge fluctuations and resulting wakefield effects, or RF power fluctuations leading to dispersive orbit jitter, can be analysed in this way.

In order to perform model independent analysis a large set of BPM data vectors $\hat{\vec{b}}_p$ for each measured pulse p is needed. The average orbit is subtracted and the individual vectors are normalized by the square root of $M \cdot P$, i.e.

$$\vec{b}_p = (\hat{\vec{b}}_p - < \hat{\vec{b}} >)/\sqrt{PM}. \tag{1}$$

These normalized difference vectors are arranged row-wise in an orbit matrix that contains finally P rows according to the number of measured pulses, and M columns according to the number of BPM's in the beamline. Normally the number of pulses is much larger than the number of BPM's. From this BPM matrix $\mathbf{B}$ one can build a

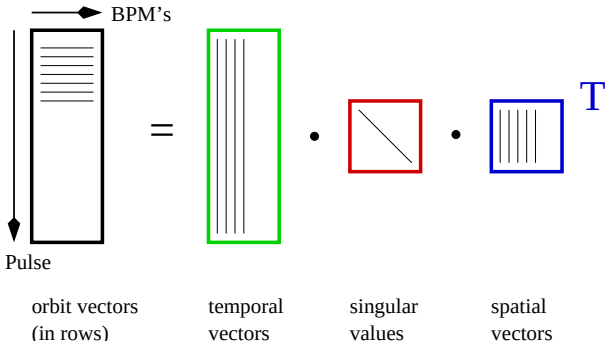

Figure 1: Schematic singular value decomposition of a BPM matrix (left).

quadratic matrix $\mathbf{B^T B}$ with the dimension M. It is now possible to compute eigenvectors and eigenvalues for the quadratic matrix.

$$(\mathbf{B^T B}) \cdot \mathbf{V} \quad = \quad \mathbf{V}\sigma \tag{2}$$

Here $\mathbf{V}$ contains the eigenvectors in columns and σ is a diagonal matrix that contains the eigenvalues.

It turns out that the eigenvectors of the matrix $\mathbf{B^T B}$ point into the direction of linear independent modes of orbit jitter. The M dimensional vector space is spanned by the BPM's. The eigenvalues are given by the mean squared jitter amplitudes averaged over space (BPM's) and time (pulses). The eigenvectors with the largest corresponding eigenvalues are the prominent jitter modes. Numerical algorithms for the computation of eigenvectors and eigenvalues commonly sort their output for descending eigenvalues [2].

The eigenvectors obtained in the described way are called spatial vectors since they describe orbit patterns along the beamline. It is also possible to perform the same procedure with the matrix $\mathbf{BB^T}$ [1]. Here one obtains temporal vectors which describe the time development of the corresponding orbit patterns.

Both types of vectors, the temporal and spatial ones can be obtained in one computational step by a singular value decomposition (SVD) of the BPM matrix $\mathbf{B}$. The SVD is shown schematically in Fig. 1.

$$\mathbf{B} \quad = \quad \mathbf{U} \cdot \mathbf{\Lambda} \cdot \mathbf{V^T}$$

$$\text{with :} \quad \begin{array}{rcl} \mathbf{U^T U} & = & \mathbf{1} \\ \mathbf{V^T V} & = & \mathbf{1} \end{array} \quad \text{, and} \quad \mathbf{\Lambda} = \begin{bmatrix} \lambda_1 & 0 & . \\ 0 & \lambda_2 & . \\ . & . & \lambda_m \end{bmatrix} \tag{3}$$

Comparing (2) and (3) it can be shown that the correct eigenvector matrices $\mathbf{V}$ (spatial) and $\mathbf{U}$ (temporal) are obtained by computing $\mathbf{B^T B}$, $\mathbf{BB^T}$ and using the properties of $\mathbf{V}$ and $\mathbf{U}$. Furthermore we identify the eigenvalue matrix $\sigma = \mathbf{\Lambda^2}$. The numbers in $\mathbf{\Lambda}$ are called singular values and are equal to the rms jitter amplitudes of the individual modes, averaged over BPM's and pulses.

[1] Although the matrix $\mathbf{BB^T}$ has P eigenvectors there are only M of them meaningful.

It is very important to realize at this point that the SVD produces *orthogonal orbit patterns* which are not necessarily connected to the underlying physical processes. In general each of the vectors is a linear combination of physical vectors. Very often, however, one process is dominating, and so the first spatial vector can be identified as caused by a unique physical process. An example for this situation are the measurements at TTF, where the orbit jitter is dominated by energy jitter of the beam.

In the general case the individual jitter modes in the machine (transverse modes, energy, phase etc.) are linear combinations of the orthogonal spatial vectors the SVD produces. Nevertheless one important information is contained in the set of singular values. The number of non-negligible values corresponds to the number of independent jitter sources.

2 Experimental setup

The orbit measurements were taken at the TTF (TESLA Test Facility) linac [3] built by the TESLA [4] collaboration. A schematic layout of the TTF linac is given in Fig. 2.

The undulator section consists of three modules 4.5 m long. Each module has integrated a F0D0 structure of 5 cells providing a phase advance of approximately 270°. In total 30 BPMs are installed in the undulator section, that is, one per quadrupole. The BPM's of undulator module 1 and 2 are of the antenna type and their electronics is described in [6]. In undulator module 3 there are 10 waveguide BPM's [7]. The experimental section downstream the undulator includes three stripline BPM's [5] (one located downstream the spectrometer dipole).

For the numerical examples presented in the next section we use only the 20 antenna BPM's in the modules 1 and 2, and one of the stripline BPM's in the dispersive region beyond the spectrometer dipole.

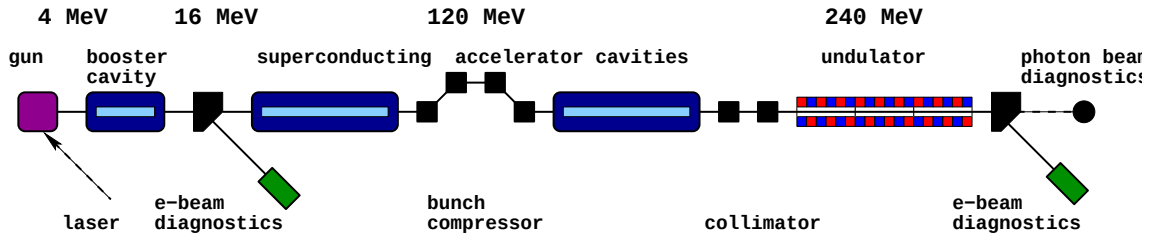

Figure 2: Schematic layout of the TTF accelerator.

3 Singular Value Spectrum and Orbit Patterns

We consider now two examples for the analysis of real data from TTF. The two examples cover different ranges of bunch charges. In the first example lower bunch charges in the range of $1 \ldots 1.5\,\mathrm{nC}$ where used. The data of the second example were taken a few months later with bunch charges of $2 \ldots 3\,\mathrm{nC}$. In the meantime the BPM electronics was equipped with attenuators, such that the optimal operating range of the electronics was shifted towards higher charges. By applying charge filters the first data set was reduced from 1601 pulses to 985, and the second one from 999 to 508. The SVD of the resulting BPM matrix with an approximate dimension 1000×20 takes about half a second on a 500 MHz Pentium processor. Only horizontal orbit measurements are considered in the examples.

The first five temporal and spatial vectors are shown for the first data set in Fig. 3. The vectors are sorted according to descent singular values. Consequently the first mode is the strongest one and it is obviously dominated by energy jitter in the machine. The amplitude of this mode is small at all BPM's, except at the last one which has the strongest dispersion. The vectors produced by the SVD are normalized in length and therefore the amplitude at the last BPM is close to 1. The time averaged jitter amplitude of the mode at the individual BPM's is obtained by multiplying the corresponding singular value with the spatial vector. The typical singular value spectrum is shown in Fig. 4. For the first mode we find $\Delta x_{\mathrm{rms}} \approx 350\,\mu\mathrm{m}$ at the last BPM. With a dispersion function of $\eta_x = 1.3\,\mathrm{m}$ we obtain a relative energy jitter (or drift) of $3 \cdot 10^{-4}$. It is interesting to look at the first temporal vector which contains basically the time evolution of the first mode, and as we now know this reflects the beam energy. The vector shows a systematic drift of the energy. In order to analyse the effect of the energy jitter in more detail the calculation was performed with and without this BPM in the matrix. For both cases the singular values are plotted in Fig. 4. For the case without the dispersive BPM one notes for both data sets that indeed the number of significant singular values above the noise floor is reduced by one. The spectrum of the other (non-dispersion) modes is slightly affected when the dispersive BPM is removed. Some fraction of the energy jitter has been attributed to other modes when the last BPM is missing. This is not surprising since the dispersion function in a bend-free section behaves exactly like a free betatron oscillation. The algorithm separates the effects better with the stronger energy signal contained in the data.

In this context it is also interesting to take a closer look at the orbit pattern of the first spatial vector in the undulator region. The orbit pattern of the first mode can be converted into residual dispersion by scaling it such that the known nominal value is reached at the last BPM. The curve is shown in Fig. 5.

The other singular values of data set 1 are already smaller by more than an order of magnitude as compared to the first one. The interpretation of the corresponding orbit patterns is not obvious, although the vectors 2 and 5 look like betatron oscillations.

For data set 2 the energy jitter deduced from the first eigenvalue seems to be much smaller ($< 3 \cdot 10^{-5}$). We note from the eigenvalue spectrum there are only three values above the noise level. Furthermore the first value is not significantly larger than the other ones which means that the corresponding vector does probably not represent a

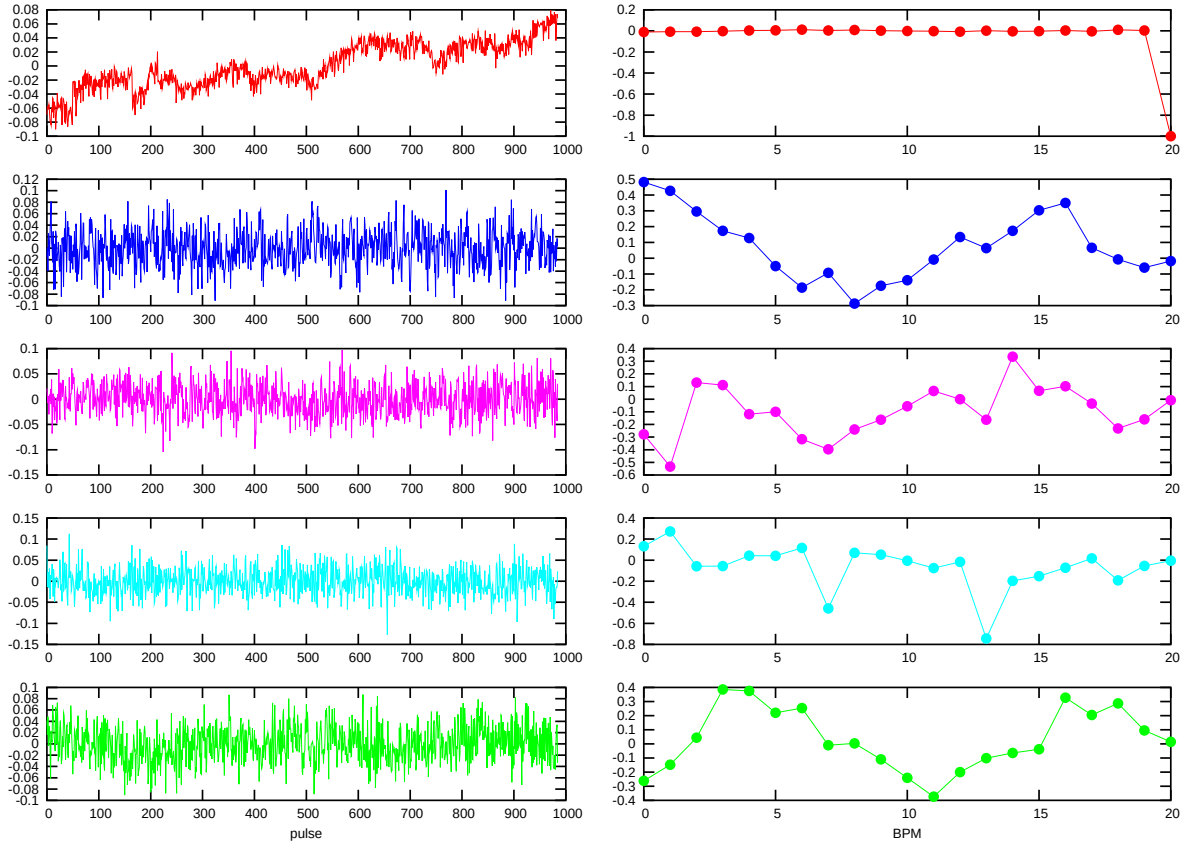

Figure 3: The first five temporal (left) and spatial (right) vectors.

pure dispersion function but is a linear combination of dispersion function and betatron oscillations.

The last singular value for data set 2 is remarkably small which is a result of the fact that one BPM was not connected to the electronics, such that we see only electrical noise. It demonstrates, however, that such kinds of failures can easily be identified by examining the singular value spectrum.

4 Resolution of the BPM's

The total measured RMS orbit jitter, averaged over pulses and BPM's is given by the quadrature sum of all singular values. As discussed above the dominating singular values are caused by the jitter of underlying physical variables. This jitter is simultaneously observed at different BPM's, i.e. correlated beam motions are detected. Noise from the BPM's themself, or the BPM electronics is usually uncorrelated. The noise amplitude can be extracted by quadratically summing up the insignificant singular values (noise floor) from Fig. 4. Since the number of significant values is normally small compared to the number of BPM's it holds approximately for the BPM resolution:

$$\sigma_{\mathrm{res}} = \left(\sum \lambda^2_{\mathrm{insignfct}}\right)^{1/2} \approx \sqrt{M} \;\cdot\; \overline{\lambda_{\mathrm{insignfct}}} \tag{4}$$

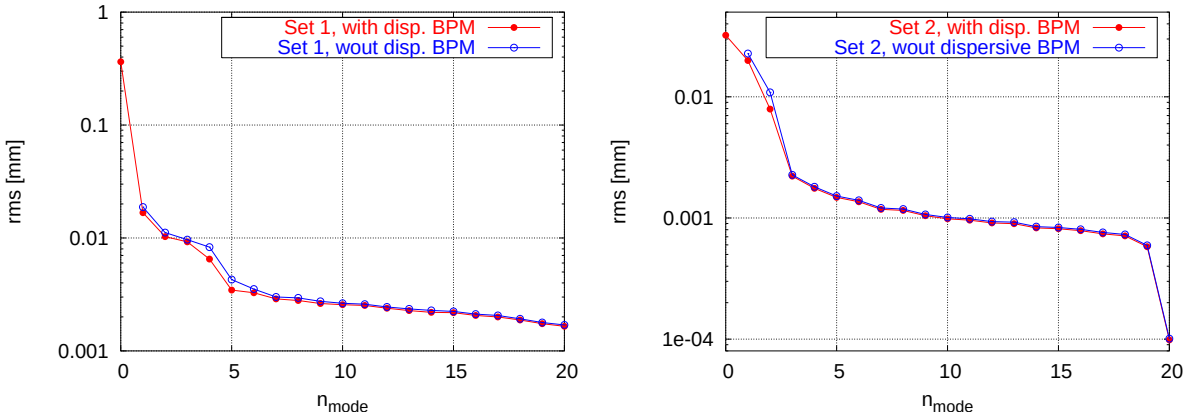

Figure 4: Singular value spectrum with and without the BPM in the dispersive region.

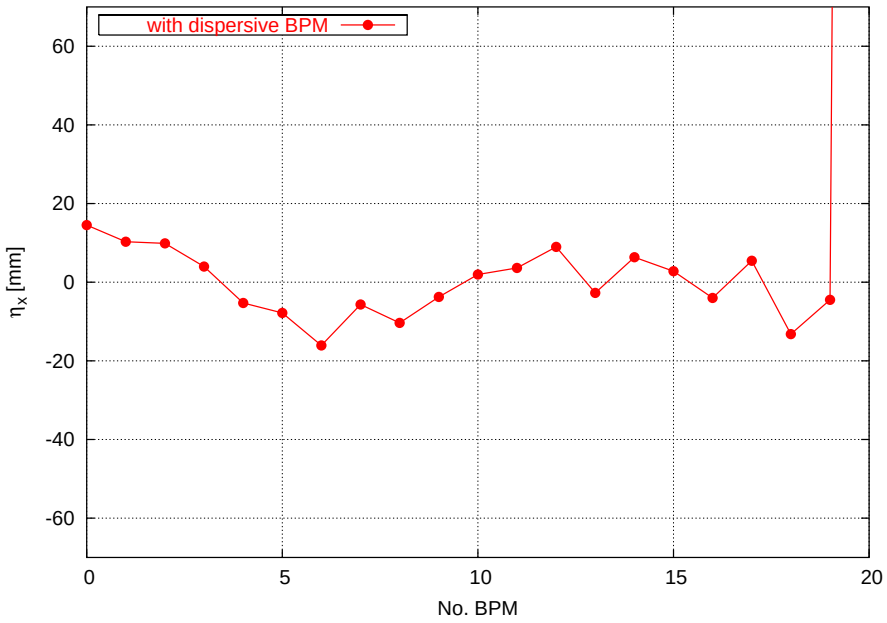

Figure 5: Residual dispersion function (deduced from the first spatial vector) in the undulator region.

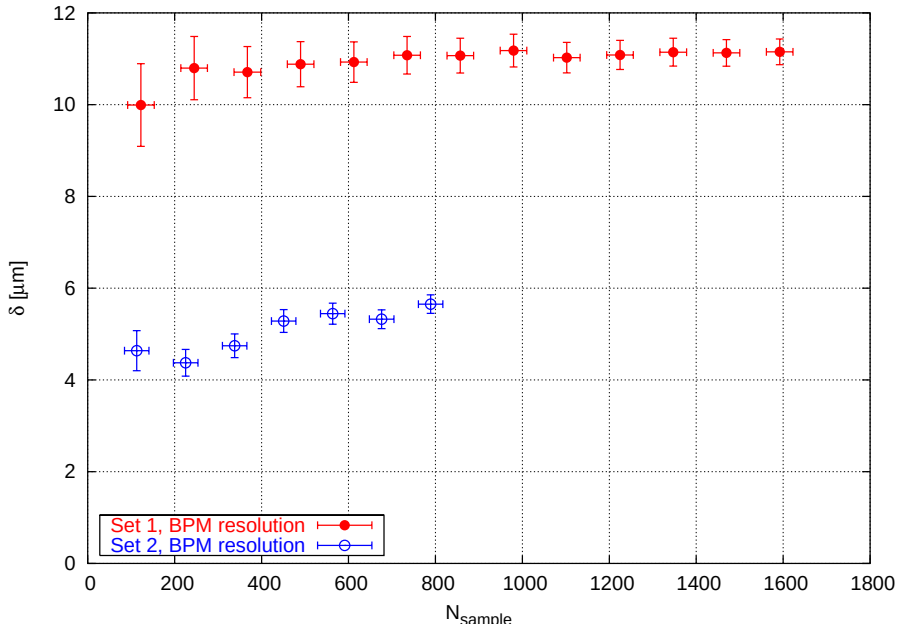

Figure 6: Computed BPM resolution as a function of the sample size.

Note that in equation (1) we normalized all BPM - vectors by $\sqrt{MP}$ and now we multiplied the singular values back by $\sqrt{M}$ to obtain the resolution of a (typical) BPM. If this normalization is correct we should obtain the same BPM resolutions for different sample sizes. In Fig. 6 the above procedure has been performed for randomly selected sub-samples with different sizes. We find that the estimated BPM resolution does not vary significantly with the sample size, as expected.

A different question is how the BPM resolution depends on the bunch charge. Since the bunch charge varies significantly within the measured data sample one can filter out different charge bins and repeat the analysis for those bunch charges. The result is shown in Fig. 7.

Indeed we find some correlation of the BPM resolution with the bunch charge. For data set 1 the resolution for charges below 0.9 nC is about 50% lower than for charges above 1.1 nC. Note that the second data set was taken with stronger signal attenuation as discussed above. For charges above 3 nC the resolution becomes worse again, an effect which is related to saturation of the BPM electronics.

5 Identification of Erroneous or Saturated BPM's

BPM's that show an unusually large uncorrelated noise will cause the appearance of a spatial vector that is close to 1 at the noisy BPM and practically zero elsewhere. Such an eigenvector is often a clear indication for a bad or saturated BPM. As an example we show measurements from the 20'th BPM in Fig. 8. This BPM saturates for bunch charges above ≈ 3 nC (which were filtered out in the previous examples) and shows "random" readouts above this value. The figure shows beam position vs. charge and the corresponding eigenvector.

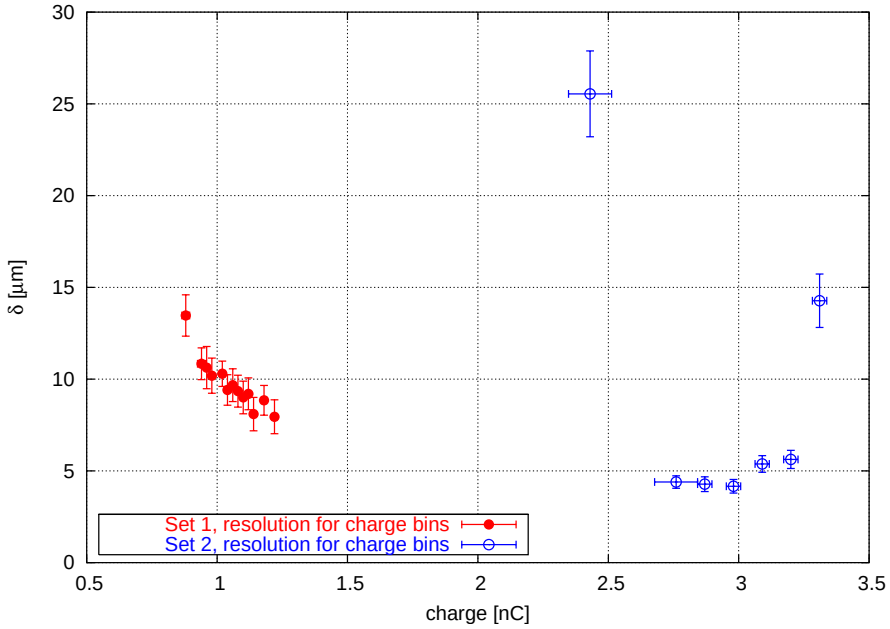

Figure 7: BPM resolution as a function of bunch charge.

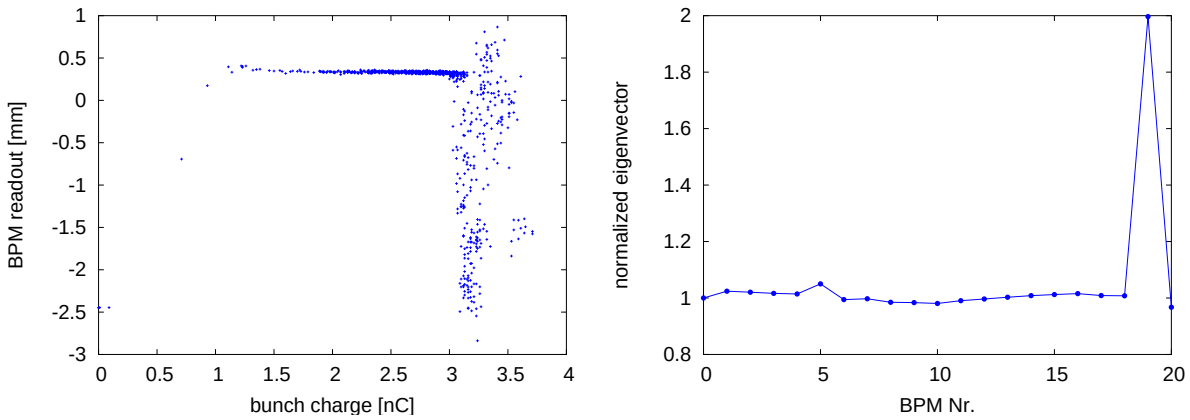

Figure 8: Position readout vs. bunch charge for BPM Nr. 20 (left), and the eigenvector caused by the noisy behavior of the BPM.

6 Conclusion

Using Model Independent Analysis (MIA) it is possible to analyze the natural orbit jitter in TTF to extract data of practical interest. As an example we show the determination of the residual dispersion function in the undulator region. We obtain typical values of $\eta_x \leq 15\,\mathrm{mm}$. By determining the uncorrelated part of measured orbit jitter at the individual BPM's in the undulator, one can extract the noise limited resolution of the BPM's. For the present electronic setup and bunch charges above 2.5 nC the resolution is better than $5\,\mu\mathrm{m}$.

References

[1] J. Irwin *et al.*, "Model-independent beam dynamics analysis," Phys. Rev. Lett. **82**, 1684 (1999). [SLAC Document Server] 1

[2] W.H. Press et al., Numerical Recipes in C, Cambridge University Press (1992). [Numerical recipes homepage: www.nr.com] 2

[3] D.A. Edwards (Ed.), TESLA Test Facility Linac - Design Report, TESLA 95-01 (1995). 3

[4] R. Brinkmann (ed) et al, TESLA Technical Design Report (2000); [Weblink] 3

[5] M. Castellano et al, TTF Stripline Readout System, EPAC 96, Sitges, Spain; [Weblink] 3

[6] M. Wendt, BPM Read-out Electronics Bases on the Broadband AM/PM Normalisation Scheme; DIPAC 2001 Proceedings, ESRF, Grenoble, May 2001; [Weblink] 3

[7] R. Lorenz et al, Beam Position Monitors inside the FEL Undulator of the TTF Linac, PAC 97, Vancouver; [Weblink] 3